Magnetic-Field-Sensing-Based Approach for Current Reconstruction, Sag Detection, and Inclination Detection for Overhead Transmission System

Qi Xu [1], Xuyang Liu [1], Ke Zhu [1], Philip W. T. Pong [1], and Chunhua Liu [2]

[1]Department of Electrical and Electronic Engineering, The University of Hong Kong, Hong Kong
[2]School of Energy and Environment, City University of Hong Kong, Hong Kong

Noncontact monitoring technique of mechanical and electrical states is increasingly attractive for the overhead transmission system. This paper proposes a new technique to detect the tower inclination and transmission line sag, and measure transmission current simultaneously. The key of this technique is to use the ground magnetoresistive (MR) sensor to measure the magnetic flux density along the center line from the three-phase transmission lines. Moreover, the magnetic field (MF) calculation formulas for a tilted tower are given in this paper. Finally, with MF calculation formulas, an algorithm based on artificial immune system (AIS) is applied to estimate the transmission line sag and tower tilt angles, and reconstruct currents. Model simulations of an overhead transmission system are carried out to verify the idea. The simulation results validate the feasibility of this noncontact approach to estimate mechanical parameters and reconstruct electrical parameters for overhead transmission system.

Index Terms— **Current reconstruction, magnetic field (MF) sensing, overhead transmission system, sagging, tower inclination.**

I. Introduction

NOWADAYS, the stability of power systems is a critical issue of concern. Due to the lack of monitoring states of power systems, potential blackouts (e.g., 2003 major blackouts in North America and Europe [1]) could happen again. These would cause tremendous economic loss and millions of consumers to lose power supply. Actually, there are overhead and underground high-voltage transmission lines (HVTLs) for the high-voltage power transmission in a power system. Overhead HVTLs account for a large percentage in transmission system compared with underground HVTLs. For example, the total length of overhead HVTLs is more than 18 $\times$ that of underground HVTLs in the U.K. [2]. Hence, a well-performed overhead HVTL monitoring system is needed to ensure power systems operate properly.

Traditionally, electrical parameters such as current [3] and voltage [4] are mainly monitored in an overhead transmission system to identify fault line. However, some power failures are caused by mechanical faults instead of electrical faults, since transmission lines are vulnerable to malicious attacks and natural hazards [5]. For example, the high temperature in scorching weather would result in elongation of transmission lines that increases sag. Bigger sag reduces clearance which makes short circuit with vegetation more likely to happen. Also, natural disasters like earthquake and typhoon can result in mechanical disturbances, especially tower inclination, and subsequently cause electrical faults like open circuit. So, both electrical and mechanical information are essential for an overhead transmission monitoring system.

Manuscript received November 5, 2018; accepted March 6, 2019. Corresponding authors: P. W. T. Pong and C. Liu (e-mail: ppong@eee.hku.hk; chunliu@cityu.edu.hk).

Color versions of one or more of the figures in this paper are available online at http://ieeexplore.ieee.org.

Digital Object Identifier 10.1109/TMAG.2019.2905567

Previous research usually applied three individual principles to measure currents, transmission line sag, and tower inclination, which lead to high construction costs and maintenance difficulty for the overhead transmission system. One conventional way to measure currents is to use current transformers (CTs), but the insulation problem cannot be neglected [6]. With a higher voltage level, the cost of insulation of CTs is increasingly more expensive. Ordinary insulation methods are unable to satisfy insulation demand at an ultrahigh voltage level. As to the mechanical parameter estimation, methods based on various principles are used to estimate the sag and tower inclination. In [7], it proposed an algorithm to estimate the sag based on on-line voltage and currents phasors. This algorithm succeeded in reducing measurement errors, and thus, estimation accuracy was improved. However, many preconditions are needed such as line resistance, the weight of conductor per unit length, and horizontal tension to estimate one mechanical parameter sag. One direct way to measure the sag is to install a GPS receiver on the conductor in the air [8]. But, it is not easy to apply in the overhead transmission system due to the high cost and trouble of GPS receiver with installation high in the sky. The measurement of the sag can also be obtained by installing inclinometer on the wire called the power line sag monitor [9]. However, this sag monitor suffers from the same trouble of installation with GPS receiver. On the other hand, dual-axis tilt sensors can directly measure the angle of tower inclination [10] in vertical and horizontal directions. However, redundant methods are indispensable for sag and current estimation. So, such situation stimulates the research of developing a real-time transmission monitoring system based on a simple mechanism to measure currents, sag, and tower inclination simultaneously.

Recently, non-intrusive detection based on MR sensors attracts more attention due to numerous advantages of MR sensors [11], [12], such as the low power consumption,

high detection accuracy, wide operating range, and cost reduction. MR sensing technology is applied in many fields, such as velocity measurement of motors [13] and fault line detection of transmission lines [14]. In the field of transmission monitoring system, a technology based on magnetic-field sensing realizes reconstruction of current, sag, and gallop [15]. However, a total of 45 sensors are required. Meanwhile, the set of these sensors are hard to install due to the distribution of those sensors especially the vertical sensor array. Another technology to estimate current and sag is developed, in which three sensors are placed at support tower to achieve the measurement [16], but it may not obtain convergence when sag decreases caused by towers tilting. It is because sag is increased every time in algorithm iteration without considering the situation of sag decrease in their proposed algorithm.

In this paper, a magnetic-field-sensing-based technique is proposed to achieve the abovementioned purposes simultaneously including the sag, tower inclination, and current detection for the overhead transmission system. This technique is realized by detecting the magnetic field (MF) distribution along the center line on the ground level so that it avoids the trouble of installation on the support towers.

II. Modeling of Testing System

The MF calculation formulas are given in this section. One typical configuration of overhead transmission lines as shown in Fig. 1 is considered in the following formula derivation since MF distribution around three transmission lines is influenced by catenaries' shapes and their relative positions. Other configurations are easy to apply formulas with a slight adaptation. In addition, it is assumed that sags of three-phase transmission lines are identical to simplify the calculation of MF distribution due to their similar surrounding environment. Only formulations of magnetic flux density generated by transmission line B in Fig. 1(a) is shown then, and the superposition principle can be used to calculate magnetic flux density generated by three-phase lines.

A. Definitions

A Cartesian coordinate system is adopted in Fig. 1(a). A simplified diagram of the Cartesian coordinate system is shown in Fig. 1(c). Assume that the left tower in Fig. 1(c) tilts. Two angles in Fig. 1(d), α and β, determine the inclination degree of a tower. α is the angle between the y-axis and the projection of a tower onto the x-y plane. β is the angle between the y-axis and the projection of a tower onto the z-y plane.

B. Magnetic Flux Density From Transmission Line B

While the shape of transmission lines is a hyperbolic cosine, one can use a parabolic approximation to describe transmission line curve for practical purpose [17]. The approximations of the catenary equation are given in [18] with transmission line B in the xy plane and distributed symmetrically with respect to the y-axis

$$\begin{cases} y = ax^2 + h \\ a = \frac{4s}{L^2} \end{cases} \tag{1}$$

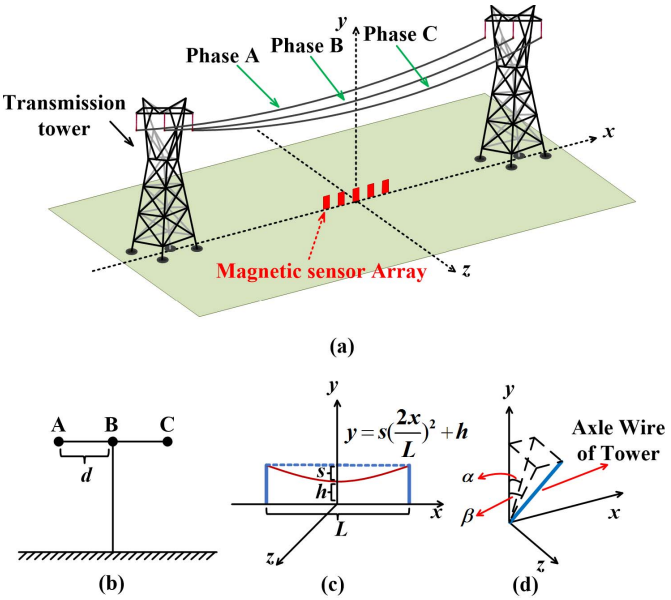

Fig. 1. Diagram of the overhead transmission lines. (a) Diagram of the transmission line coordinate system. (b) One possible configuration of overhead transmission lines. d is the distance between two adjacent transmissions lines. (c) Simplified diagram of transmission line B in the xyz coordinate system. Blue solid lines represent power transmission towers with no tilt. The red line represents transmission line B. (d) Tower tilt diagram.

where s is the sag, h is the height of the lowest point from the ground, and L is the distance of two adjacent towers.

Biot–Savart law is applied to calculate the magnetic flux density from transmission line B in [18]. The equations of the MF at a point (x_0, y_0, and z_0) in space from transmission line B in one span are adapted as follows:

$$\begin{cases} B_0 = \mu_0 \int_{-L/2}^{L/2} (J_x \mathbf{a_x} + J_y \mathbf{a_y} + J_z \mathbf{a_z}) dx \\ J_x = \dfrac{I_i 2a z_0 x}{4\pi d_i} \\ J_y = -\dfrac{I_i z_0}{4\pi d_i} \\ J_z = \dfrac{I_i (ax^2 - 2ax_0 x + y_0 - h)}{4\pi d_i} \\ d_i = [(x - x_0)^2 + z_0^2 + (y_0 - ax^2 - h)^2]^{3/2} \end{cases} \tag{2}$$

where I_i is the current in transmission line B.

However, it would be rather difficult to determine the transmission line and MF equations when the tower tilts because the z values of a single transmission line are not the same in xyz coordinate system. Even though the equations are worked out, it can be imagined that equations would be very complex. One possible way to solve this problem is to conduct geometric transformation [19]. Geometric transformation mapping points to points may not make equations less complicated. Thus, the coordinate system in Fig. 1(a) needs to be transformed to simplify equations. Two principles are applied to transform the original coordinate system.

1) Ensure that transmission line i is in the x_i-y_i plane in the $x_i y_i z_i$ coordinate system. (i = A, B, and C).
2) Ensure that the xz plane and x_i-z_i plane share the same plane. (i = A, B, and C).

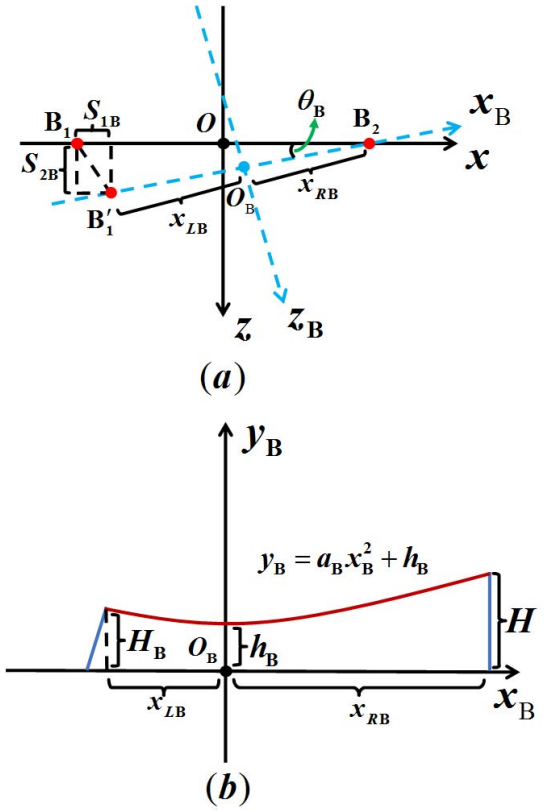

Fig. 2. Diagram of the *xyz* coordinate system transformation.(a) *xyz* coordinate system transformation on the *xy* plane. (b) Shape of transmission line B in the $x_{\mathrm{B}}y_{\mathrm{B}}z_{\mathrm{B}}$ coordinate system.

Fig. 2 shows how the $x_{\mathrm{B}}y_{\mathrm{B}}z_{\mathrm{B}}$ coordinate system is built. In Fig. 2(a), B_1 and B_2 are the projections of suspension points of transmission line B onto the *xy* plane before tilting. B_1' is the projection of the suspension point of transmission line B onto the *xy* plane after tilting. $x_{\mathrm{B}}y_{\mathrm{B}}z_{\mathrm{B}}$ is the new coordinate system built after tilting while the y_{B}-axis remains vertical to the ground and O_{B} is the projection of the lowest point of transmission line B onto the *xz* plane after tilting. In Fig. 2(b), solid blue lines represent power transmission towers after tilting, the red line represents transmission line B, h_{B} is the height of the lowest point after tilting, H is the height of suspension points before tilting, and H_{B} is the height of the tilted suspension point of transmission line B. After the tower inclination, it is clear that the shape equation of transmission line B changes. In addition, the range of integration (from $-L/2$ to $L/2$), h, and the point (x_0, y_0, and z_0) in (2) also change. Section III will talk about how to calculate the changes of the shape of transmission line B, the integration range, h, and the point (x_0, y_0, and z_0).

From the geometrical relationship in Fig. 2, some quantities can be easily obtained as follows:

$$\begin{cases} S_{1\mathrm{B}} = H_{\mathrm{B}} \tan\alpha \\ S_{2\mathrm{B}} = H_{\mathrm{B}} \tan\beta \\ \tan\theta_{\mathrm{B}} = \frac{S_{2\mathrm{B}}}{L - S_{1\mathrm{B}}} \\ H_{\mathrm{B}}^2 + S_{1\mathrm{B}}^2 + S_{2\mathrm{B}}^2 = H^2. \end{cases} \tag{3}$$

Since the shape of the line relative to the lowest point is unaffected by the tower inclination [5], the parabolic shape can still represent transmission line B in the $x_{\mathrm{B}}y_{\mathrm{B}}z_{\mathrm{B}}$ coordinate system, which is expressed as

$$y_{\mathrm{B}} = a_{\mathrm{B}}x_{\mathrm{B}}^2 + h_{\mathrm{B}} \tag{4}$$

where x_{LB}, x_{RB}, and h_{B} in Fig. 2 and a_{B} need to be determined in order to use (2). Four equations are used to obtain them

$$\begin{cases} a_{\mathrm{B}}x_{LB}^2 + h_{\mathrm{B}} = H_{\mathrm{B}} \\ a_{\mathrm{B}}x_{RB}^2 + h_{\mathrm{B}} = H \\ (x_{LB} + x_{RB})^2 = (L - S_{1\mathrm{B}})^2 + S_{2\mathrm{B}}^2 \\ \int_{-\frac{L}{2}}^{\frac{L}{2}} y ds = \int_{-x_{LB}}^{x_{RB}} y_{\mathrm{B}} ds. \end{cases} \tag{5}$$

The fourth equation in (5) means that the length of transmission line B remains the same before and after the tower tilts.

In order to conduct the coordinate system transformation, the coordinate of the origin O_{B} can be deduced by using similar triangle calculations in Fig. 2(a)

$$\frac{x_{RB}}{x_{LB} + x_{RB}} = \frac{\frac{L}{2} - x(O_{\mathrm{B}})}{L - S_{1\mathrm{B}}} = \frac{z(O_{\mathrm{B}})}{S_{2\mathrm{B}}}. \tag{6}$$

Here, [$x(O_{\mathrm{B}})$, $y(O_{\mathrm{B}})$, and $z(O_{\mathrm{B}})$] is the coordinate of O_{B} in the *xyz* coordinate system. Since the *xz* plane and x_{B}-z_{B} plane are on the same plane, $y(O_B)$ is zero.

Once $\tan\theta_{\mathrm{B}}$ and the coordinate of the origin O_{B} are obtained, the $x_{\mathrm{B}}y_{\mathrm{B}}z_{\mathrm{B}}$ coordinate system can be built accordingly. Then, ($x_{0\mathrm{B}}$, $y_{0\mathrm{B}}$, and $z_{0\mathrm{B}}$), which is the coordinate in the $x_{\mathrm{B}}y_{\mathrm{B}}z_{\mathrm{B}}$ coordinate system of any point (x_0, y_0, and z_0) in the *xyz* coordinate system, can be calculated. $y_{0\mathrm{B}}$ is equal to y_0. $x_{0\mathrm{B}}$ and $z_{0\mathrm{B}}$ are calculated by

$$\begin{cases} x_{0\mathrm{B}} = r\cos\varphi \\ z_{0\mathrm{B}} = r\sin\varphi \\ r = \sqrt{[x_0 - x(O_{\mathrm{B}})]^2 + [z_0 - z(O_{\mathrm{B}})]^2} \\ \varphi = \arctan\frac{z_0 - z(O_{\mathrm{B}})}{x_0 - x(O_{\mathrm{B}})} + \theta_{\mathrm{B}}. \end{cases} \tag{7}$$

Thus, the point (x_0, y_0, and z_0) is now ($r\cos\varphi$, y_0, and $r\sin\varphi$) in the $x_{\mathrm{B}}y_{\mathrm{B}}z_{\mathrm{B}}$ coordinate system.

Consequently, with all parameters needed, the magnetic flux density at point ($x_{0\mathrm{B}}$, $y_{0\mathrm{B}}$, and $z_{0\mathrm{B}}$) in the $x_{\mathrm{B}}y_{\mathrm{B}}z_{\mathrm{B}}$ coordinate system can be determined by adapting (2). According to Fig. 3, the magnetic flux density in the $x_{\mathrm{B}}y_{\mathrm{B}}z_{\mathrm{B}}$ coordinate system is

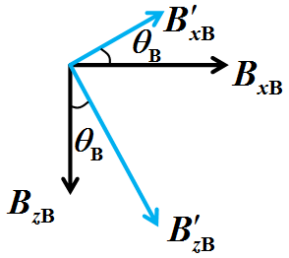

Fig. 3. Transformation of magnetic flux density generated by transmission line B.

transformed to that in the xyz coordinate system

$$\begin{cases} B_{x\mathrm{B}} = B'_{x\mathrm{B}} \cos\theta_{\mathrm{B}} + B'_{z\mathrm{B}} \sin\theta_{\mathrm{B}} \\ B_{y\mathrm{B}} = B'_{y\mathrm{B}} \\ B_{z\mathrm{B}} = -B'_{x\mathrm{B}} \sin\theta_{\mathrm{B}} + B'_{z\mathrm{B}} \cos\theta_{\mathrm{B}} \end{cases} \tag{8}$$

where ($B_{x\mathrm{B}}$, $B_{y\mathrm{B}}$, and $B_{z\mathrm{B}}$) is the magnetic flux density at point (x_0, y_0, and z_0) in the xyz coordinate system from transmission line B, and ($B'_{x\mathrm{B}}$, $B'_{y\mathrm{B}}$, $B'_{z\mathrm{B}}$) is the magnetic flux density at point ($x_{0\mathrm{B}}$, $y_{0\mathrm{B}}$, and $z_{0\mathrm{B}}$) in the $x_{\mathrm{B}}y_{\mathrm{B}}z_{\mathrm{B}}$ coordinate system from transmission line B.

Calculations of magnetic flux density generated by transmission line A and C in the xyz coordinate system are similar except that some parameters are calculated by slightly different equations. The detailed changes of formulas for transmission line A and C are described in the Appendix.

Finally, three components are added to get the total magnetic flux density generated by transmission line A, B, and C in the xyz coordinate system

$$\begin{cases} B_x = B_{x\mathrm{A}} + B_{x\mathrm{B}} + B_{x\mathrm{C}} \\ B_y = B_{y\mathrm{A}} + B_{y\mathrm{B}} + B_{y\mathrm{C}} \\ B_z = B_{z\mathrm{A}} + B_{z\mathrm{B}} + B_{z\mathrm{C}} \end{cases} \tag{9}$$

where (B_x, B_y, and B_z) is the total magnetic flux density generated by transmission line A, B, and C at point (x_0, y_0, and z_0) in the xyz coordinate system.

III. Magnetic-Field-Sensing-Based Approach for Monitoring Overhead Transmission System

The novelty of our approach is that the y and z components of magnetic flux densities (B_y and B_z) at five points along the x-axis are capable of estimating transmission line sag and tower tilt angles. With these estimated parameters, currents in three phases can be reconstructed precisely.

Since these three parameters (α, β, and sag) have influences on y and z components of magnetic flux density (B) in different ways, measuring B_y and B_z is enough to estimate α, β, and sag. MF distribution is simulated in one situation where $L = 100$ m, $d = 10$ m, $s + h = 20$ m, frequency of 50 Hz, and currents of 1 kA per phase in Fig. 1. Emulations are studied when one of the parameters changes. α, β, and sag are distinguished in three aspects: the amplitude and phase of B, and the position (P_{MAX}) of maximum B along the x-axis.

Only impacts of α, β, and sag on B_z along the x-axis are shown because impacts onB_y and B_z are similar. The origin is a typical point to show influences caused by mechanical changes. Figs. 4 and 5 show that α, β, and sag individually affect B_z at point (0, 0, 0) and P_{MAX}. From Fig. 4, α and sag change the amplitude of B_z with no phase shifting, while various β lead to phase shifting but negligible effect on the amplitude of B_z. From Fig. 5, P_{MAX} remains the same with a different sag but changes slightly with α. Meanwhile, α and sag keep P_{MAX} at a certain point in one current cycle. However, β changes P_{MAX} in one current cycle and appears periodic.

Because of correlations between three parameters and MF distribution, an approach for estimating three parameters is developed. In practice, the MF distribution can be measured by MR sensors. According to [15], MR sensors are sensitive enough to measure magnetic flux density under transmission

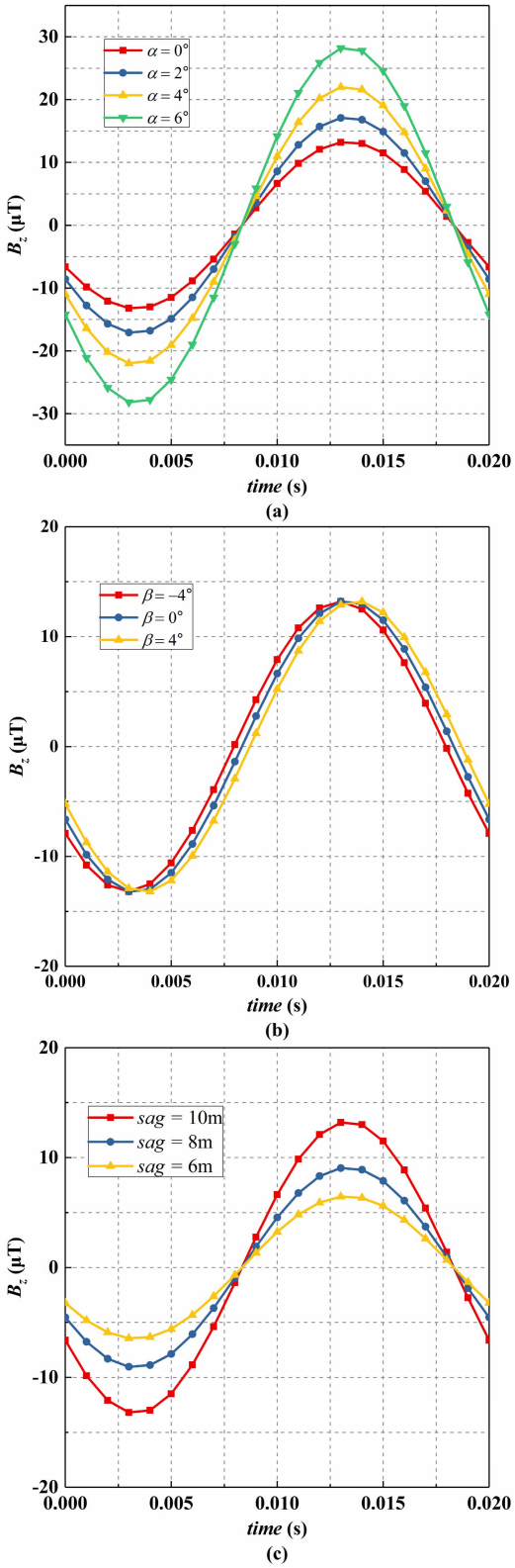

Fig. 4. (a) B_z at point (0, 0, 0) in one current cycle when α are various. (b) B_z at point (0, 0, 0) in one current cycle when β are various. (c) B_z at point (0, 0, 0) in one current cycle when sag are various.

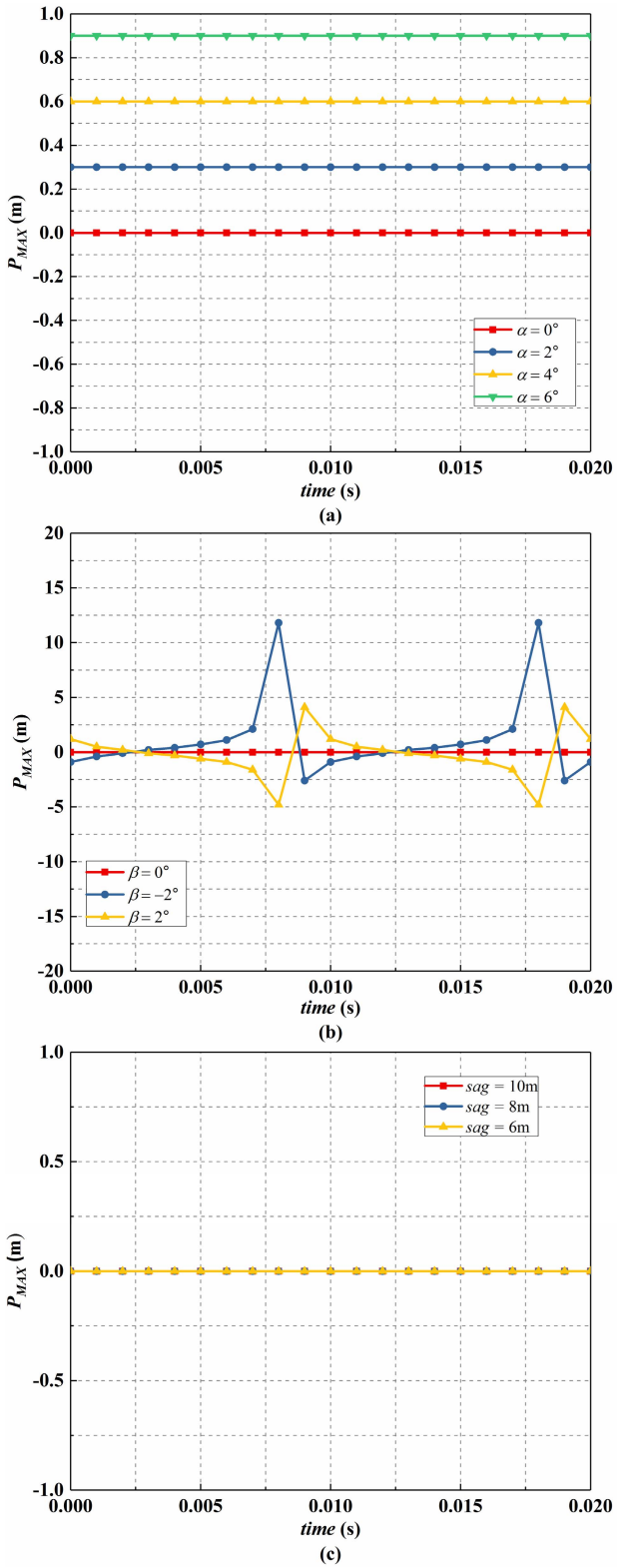

Fig. 5. (a) Position of maximum B_z along the x-axis in one current cycle when α are various. (b) Position of maximum B_z along the x-axis in one current cycle when β are various. (c) Position of maximum B_z along the x-axis in one current cycle when sag are various.

lines on the ground level. In particular, tunneling magnetoresistive (TMR) sensors are desirable for their low cost, low power consumption, and high detection accuracy [20]. With measured MF, an optimization approach based on artificial immune system (AIS) algorithm [21] is applied to obtain α, β, and sag. The whole process is shown in Fig. 6. The approach starts with the pre-stored position coefficient matrix A which is related to the positions of transmission lines. The matrix A can be obtained by MF calculation formulas in Section II and the Appendix. In the beginning, the matrix A is calculated with normal α, β, and sag. Then, the currents in three phases are calculated with the least-squares estimation method. Afterward, magnetic flux density can be deduced with these calculated currents. The total differences (Diff) between calculated and measured MF data are compared with threshold ε. If Diff exceeds ε, A will be updated by AIS algorithm. The circulation stops until Diff is less than ε.

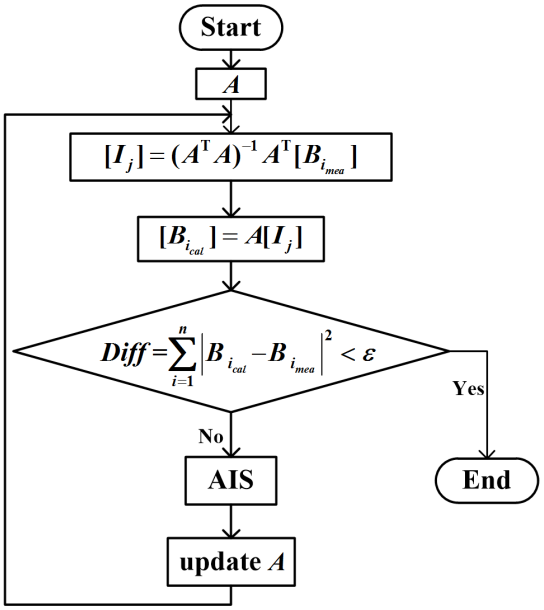

Fig. 6. Flowchart of the magnetic-field-sensing-based approach.

In our approach, an array of five dual-axis magnetic sensing points with an interval of 5 m is set along the x-axis on the ground level for easy installation. These sensing points are located right under the lowest point of transmission line B for easy measurement because of relatively large magnetic flux density there. Five sensing points' positions are (−10 m, 0, 0), (−5 m, 0, 0), (0, 0, 0), (5 m, 0, 0), and (10 m, 0, 0). Theoretically, three single-axis sensing points are enough to reconstruct currents for three phases. Five dual-axis sensing points are used for enhancing accuracy.

IV. Estimation and Reconstruction Results

The proposed approach is verified on a simulation model of an overhead transmission system in four different situations, where sag increases from 10 to 12 m, tower tilts, −10° phase shifting occurs in phase A, and current increases by 10% in phase A. In the simulation, the normal operation state of the overhead transmission system is $s = 10$ m, $\alpha = 0°$, $\beta = 0°$, $h = 10$ m, $L = 100$ m, $d = 10$ m, frequency of 50 Hz, and currents of 1 kA per phase. Table I shows the actual and reconstructed values of α, β, and sag in four situations mentioned before and proves that the reconstruction results match well with the actual values. As to the estimation

TABLE I
ACTUAL AND RECONSTRUCTED α, β, AND SAG

situation		α(°)	β(°)	sag(m)
1	Actual value	0	0	12
	Reconstructed value	0.01	-0.01	11.98
2	Actual value	5	2	10
	Reconstructed value	5.02	1.98	9.98
3	Actual value	0	0	10
	Reconstructed value	0	0	10
4	Actual value	0	0	10
	Reconstructed value	0	0	10

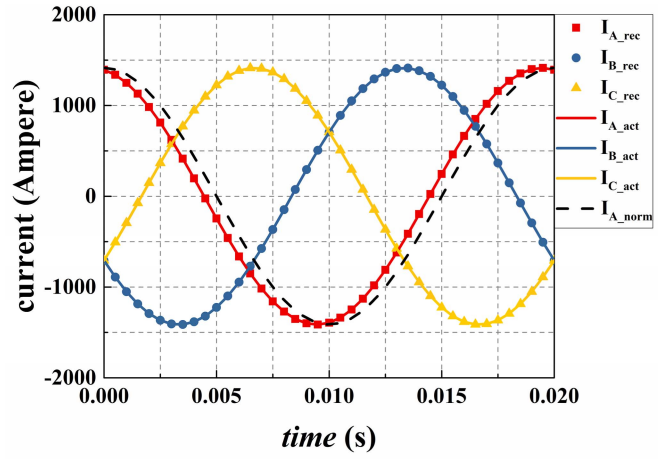

Fig. 7. Reconstructed and actual currents in three phases when −10° phase shifting occurs in phase A. The dashed line is normal current in phase A.

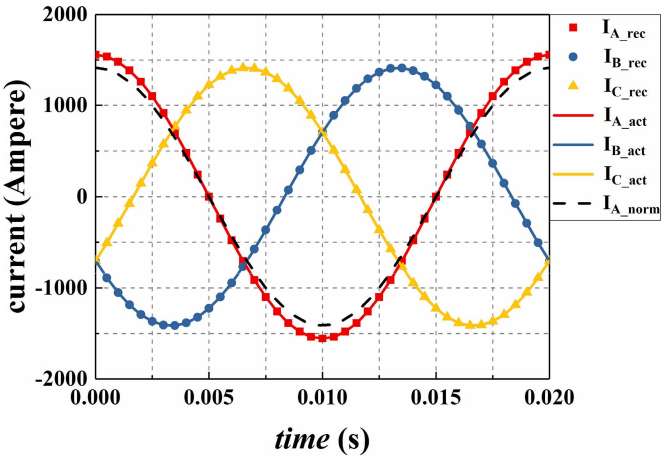

Fig. 8. Reconstructed and actual currents in three phases when 10% current imbalance occurs in phase A. The dashed line is normal current in phase A.

of α and β, errors between actual and reconstructed values are less than or equal to 0.02°. The errors of the parameter sag are less than 0.3%. With these three estimated parameters, currents in three phases are reconstructed 41× with an interval of 0.5 in 20 ms (one current cycle). Figs. 7 and 8 demonstrate that the reconstructed currents are almost identical to the actual currents when current imbalances [phase angle and root-mean-square (rms)] occur in phase A. The rms errors of currents in these two scenarios are 9.89×10^{-12} and 1.02×10^{-11} A. To summarize, the estimated α, β, and sag match well with actual values by using the proposed approach and the results of reconstructing currents are satisfactory.

V. CONCLUSION

A magnetic-field-sensing-based approach for current reconstruction, transmission line sag, and tower tilt estimation in an overhead transmission line system is proposed in this paper. This technique can monitor electrical and mechanical states of overhead transmission line system. This paper provides the MF calculation formulas with a tilted tower. Moreover, this paper studies the changes of magnetic flux density generated by three-phase transmission lines when one of these three parameters (α, β, and sag) varies. The changes of MF distribution mainly reflect in three aspects: the amplitude and phase of B, and the position (P_{MAX}) of maximum B along the x-axis. Simulation successfully validates the proposed approach in this paper. The proposed technique needs a relatively small number of measurements and estimates transmission line sag and tower inclination angles accurately while reconstructing electrical information currents with precision simultaneously. Moreover, the non-intrusive characteristic of the approach makes installation work convenient and safe in practice. Therefore, the approach is beneficial to be further incorporated into a monitoring system of a smart grid. This technique can be potentially implemented as a portable platform with TMR sensors that can measure the electrical and mechanical parameters due to its easy installation, compact size, and convenience of maintenance.

APPENDIX

For transmission line A, the changes of equations are

$$\begin{cases} S_{1\mathrm{A}} = H_{\mathrm{B}} \tan\alpha \\ S_{2\mathrm{A}} = H_{\mathrm{B}} \tan\beta - d\cos\beta \\ \tan\theta_{\mathrm{A}} = \frac{S_{2A}+d}{L-S_{1A}} \\ H_{\mathrm{A}}^2 + S_{1\mathrm{A}}^2 + S_{2\mathrm{A}}^2 = H^2 + d^2 \end{cases} \tag{10}$$

$$\begin{cases} a_{\mathrm{A}} x_{LA}^2 + h_{\mathrm{A}} = H_{\mathrm{A}} \\ a_{\mathrm{A}} x_{RA}^2 + h_{\mathrm{A}} = H \\ (x_{LA} + x_{RA})^2 = (L - S_{1\mathrm{A}})^2 + (S_{2\mathrm{A}} + d)^2 \\ \int_{-\frac{L}{2}}^{\frac{L}{2}} y ds = \int_{-x_{LA}}^{x_{RA}} y_{\mathrm{A}} ds \end{cases} \tag{11}$$

$$\frac{x_{RA}}{x_{LA}+x_{RA}} = \frac{\frac{L}{2} - x(O_{\mathrm{A}})}{L - S_{1\mathrm{A}}} = \frac{z(O_{\mathrm{A}}) + d}{S_{2\mathrm{A}} + d}. \tag{12}$$

For transmission line C, the changes of formulas are

$$\begin{cases} S_{1\mathrm{C}} = H_{\mathrm{B}} \tan\alpha \\ S_{2\mathrm{C}} = H_{\mathrm{B}} \tan\beta + d\cos\beta \\ \tan\theta_{\mathrm{C}} = \frac{S_{2C}-d}{L-S_{1C}} \\ H_{\mathrm{C}}^2 + S_{1\mathrm{C}}^2 + S_{2\mathrm{C}}^2 = H^2 + d^2 \end{cases} \tag{13}$$

$$\begin{cases} a_{\mathrm{C}} x_{LC}^2 + h_{\mathrm{C}} = H_{\mathrm{C}} \\ a_{\mathrm{C}} x_{RC}^2 + h_{\mathrm{C}} = H \\ (x_{LC} + x_{RC})^2 = (L - S_{1\mathrm{C}})^2 + (S_{2\mathrm{C}} - d)^2 \\ \int_{-\frac{L}{2}}^{\frac{L}{2}} y ds = \int_{-x_{LC}}^{x_{RC}} y_{\mathrm{C}} ds \end{cases} \tag{14}$$

$$\frac{x_{RC}}{x_{LC}+x_{RC}} = \frac{\frac{L}{2} - x(O_{\mathrm{C}})}{L - S_{1C}} = \frac{z(O_{\mathrm{C}}) - d}{S_{2\mathrm{C}} - d}. \tag{15}$$

ACKNOWLEDGMENT

This work was supported in part by the Seed Funding Program for Basic Research, Seed Funding Program for Applied Research, and Small Project Funding Program from the University of Hong Kong, ITF Tier 3 Funding under Grant ITS/203/14, Grant ITS/104/13, and Grant ITS/214/14, in part by RGC-GRF under Grant HKU 17210014 and Grant HKU 17204617, and in part by the University Grants Committee of Hong Kong under Contact AoE/P-04/08.

REFERENCES

[1] G. Andersson *et al.*, "Causes of the 2003 major grid blackouts in North America and Europe, and recommended means to improve system dynamic performance," *IEEE Trans. Power Syst.*, vol. 20, no. 4, pp. 1922–1928, Nov. 2005.

[2] *Overhead Power Lines*. Accessed: Aug. 14, 2018. [Online]. Available: http://www.emfs.info/sources/overhead/

[3] C. Yao *et al.*, "A novel lightning current monitoring system based on the differential-integral loop," *IEEE Trans. Dielectrics Electr. Insul.*, vol. 20, no. 4, pp. 1247–1255, Aug. 2013.

[4] O. Samuelsson, M. Hemmingsson, A. H. Nielsen, K. O. H. Pedersen, and J. Rasmussen, "Monitoring of power system events at transmission and distribution level," *IEEE Trans. Power Syst.*, vol. 21, no. 2, pp. 1007–1008, May 2006.

[5] S. Malhara and V. Vittal, "Mechanical state estimation of overhead transmission lines using tilt sensors," *IEEE Trans. Power Syst.*, vol. 25, no. 3, pp. 1282–1290, Aug. 2010.

[6] M. Wang, A. J. Vandermaar, and K. D. Srivastava, "Review of condition assessment of power transformers in service," *IEEE Elect. Insul. Mag.*, vol. 18, no. 6, pp. 12–25, Nov./Dec. 2002.

[7] Y. Du and Y. Liao, "On-line estimation of transmission line parameters, temperature and sag using PMU measurements," *Electr. Power Syst. Res.*, vol. 93, pp. 39–45, Dec. 2012.

[8] C. Mensah-Bonsu, U. F. Krekeler, G. T. Heydt, Y. Hoverson, J. Schilleci, and B. L. Agrawal, "Application of the Global Positioning System to the measurement of overhead power transmission conductor sag," *IEEE Trans. Power Del.*, vol. 17, no. 1, pp. 273–278, Jan. 2002.

[9] A. Nourai and R. M. Hayes, "Power line sag monitor," U.S. Patent 6 205 867, Mar. 27, 2001.

[10] Y. Hu and K. Liu, *Inspection and Monitoring Technologies of Transmission Lines with Remote Sensing*. New York, NY, USA: Academic, 2017, pp. 257–264.

[11] P. P. Freitas, R. Ferreira, S. Cardoso, and F. Cardoso, "Magnetoresistive sensors," *J. Phys. Condens. Matter*, vol. 19, pp. 1–21, 2007.

[12] L. A. Jander, C. Smith, and R. Schneide, "Magnetoresistive sensors for nondestructive evaluation," in *Proc. 10th SPIE Int. Symp. Nondestruct. Eval. Health Monit. Diagnostics*, 2005, pp. 1–14.

[13] X. Liu, C. Liu, and P. W. T. Pong, "Velocity measurement technique for permanent magnet synchronous motors through external stray magnetic field sensing," *IEEE Sensors J.*, vol. 18, no. 10, pp. 4013–4021, May 2018.

[14] K. Zhu, W. Lee, and P. W. T. Pong, "Fault-line identification of HVDC transmission lines by frequency-spectrum correlation based on capacitive coupling and magnetic field sensing," *IEEE Trans. Magn.*, vol. 54, no. 11, Nov. 2018, Art. no. 4001805.

[15] X. Sun, Q. Huang, Y. Hou, L. Jiang, and P. W. T. Pong, "Noncontact operation-state monitoring technology based on magnetic-field sensing for overhead high-voltage transmission lines," *IEEE Trans. Power Del.*, vol. 28, no. 4, pp. 2145–2153, Oct. 2013.

[16] A. H. Khawaja, Q. Huang, J. Li, and Z. Zhang, "Estimation of current and sag in overhead power transmission lines with optimized magnetic field sensor array placement," *IEEE Trans. Magn.*, vol. 53, no. 5, May 2017, Art. no. 6100210.

[17] T. O. Seppa, "Factors influencing the accuracy of high temperature sag calculations," *IEEE Trans. Power Del.*, vol. 9, no. 2, pp. 1079–1089, Apr. 1994.

[18] A. V. Mamishev, R. D. Nevels, and B. D. Russell, "Effects of conductor sag on spatial distribution of power line magnetic field," *IEEE Trans. Power Del.*, vol. 11, no. 3, pp. 1571–1576, Jul. 1996.

[19] S. Malhara and V. Vittal, "Monitoring sag and tension of a tilted transmission line using geometric transformation," in *Proc. IEEE Power Energy Soc. Gen. Meeting*, Jul. 2009, pp. 1–7.

[20] C. Duret and S. Ueno, "TMR: A new frontier for magnetic sensing," NTN-SNR ROULEMENTS Res. Innov. Mechatron., Annecy, France, Tech. Rep. 80, 2012, pp. 64–71.

[21] L. N. de Castro and J. Timmis, "An artificial immune network for multimodal function optimization," in *Proc. Congr. Evol. Comput. (CEC)*, Honolulu, HI, USA, vol. 1, May 2002, pp. 699–704.